

Determination of water permeability for cementitious materials with minimized batch effect

Zhidong Zhang, George Scherer

Department of Civil and Environmental Engineering, Princeton University, Princeton, NJ 08544, USA

Abstract

Values of water permeability for cementitious materials reported in the literature show a large scatter. This is partially attributed to the fact that materials used in different studies are different. To eliminate the effects of cements, specimen preparation, curing conditions and other batch effects, this study employs a long cylindrical cement paste to prepare all specimens for a variety of permeability determination methods, such as beam bending, sorptivity, Katz–Thompson and Kozeny–Carman equations. Permeabilities determined by these methods are then used in a moisture transport model. Compared with the measured mass loss curves, we found that permeability determined by the beam bending method provides much closer results to the measured ones than other methods. The difference results from that the saturated specimen is used in the beam bending method while specimens in other methods are dried (or rewetted). As already shown in the literature, the microstructure of the dried or rewetted specimens is altered and different to the original microstructure of the water saturated specimens. . . .

1 Introduction

The durability of concrete structures is always closely related to the moisture transport properties in cementitious materials. The liquid uptake when concrete is in contact with liquid water (e.g., groundwater, rain) can induce the penetration of aggressive agents (e.g., chloride ions) through the concrete cover. A common natural condition - drying/wetting cycles - can increase the rate of chloride ingress compared to the saturated condition [1]. Carbon dioxide may transport within the gaseous phase in concrete and decrease pH of the pore solution. All these processes are able to result in corrosion to the rebars and deterioration of concrete. For this reason, moisture transport becomes a crucial theme when evaluating the durability.

Moisture transport in partially saturated porous media such as cementitious materials is mainly governed by the transport of three phases: liquid water, water vapour and dry air. The previous studies have shown that dry air has very low contribution to the mass of moisture transport and only causes fluctuating air pressure in the material [2, 3]. This conclusion was also drawn by the asymptotic analysis performed by Coussy and Thiéry [4, 5]. In addition, considering that the liquid phase remains incompressible and total gas pressure is constant, the mass balance equations of moisture transport can be represented by a simplified equation, including only liquid water and vapour [6, 7]. Mainguy et al. [2] further simplified the model for specific conditions, by considering only liquid water and neglecting the vapour diffusion. They found that such a model can give results for simulating drying mass loss curves very similar to the multiphase model. Hence, the

transport coefficient - water permeability that governs the liquid water transport becomes extremely important. For a given material, the ideal situation to perform moisture transport simulations is that K_l is experimentally determined and then used in the moisture transport model.

In most literature, water permeability K_l with a unit of m^2 is considered as an intrinsic property of the porous material, meaning that K_l only depends on the microstructure and should be valid for other fluids. That is why in some papers K_l is named as “intrinsic” permeability (e.g., [2, 7, 8]). Nevertheless, “intrinsic” permeabilities measured by gases (oxygen and nitrogen [9]) and solvents (methanol [10] and isopropanol [11, 12]) are often found to be greater than K_l . Reasons for this will be discussed later. To avoid the confusion, in this paper, the terminology of water permeability instead of intrinsic permeability is used hereafter.

For cementitious materials, the determination of water permeability is an active research field reported in a voluminous literature. The permeability can be determined either directly by experiments or indirectly by theoretical models based on other measured data. Conventional methods to measure K_l are classified as flow-through techniques as they measure the flux under steady state condition for fully saturated specimens, with the geometry of either truncated cones [13] or cylinders/disks [14, 15, 16, 17, 18, 19, 12]. During measurements, the side of the specimen must be sealed and liquid water is injected from one face by applying extra pressure so that the outflow can be only observed on the opposite face. When the flow in the porous body reaches steady state, the flow rate is then used to calculate K_l according to Darcy’s law. These methods are not difficult to do, although they may take a long time to reach steady state flow (e.g., several weeks) for low permeable materials. To reduce the measurement time, it was suggested to increase the applied pressure [19], but this may risk altering the structure of materials and increase the water leak at the interface between the specimen and the pressure cell. Instead of applying continuous constant pressure, pressure relaxation methods involve increasing pressure on one side and observing the decrease of pressure due to liquid being pushed to another side (e.g., [20]). These methods are rapid but they still need high pressure and thus have the same problems as the other conventional flow-through methods.

Recent studies used hollow cylinders [21, 22, 23] which measured radial flow of water under applied pressure. The main advantage of this kind of method is that the total area which allows fluids flowing through is much larger than the disc specimens; therefore, the measurements showed higher accuracy and repeatability [21, 23], whilst the large area may have higher chances to face the effect of heterogeneity, which means that any cracks or area having greater water flow can significantly change the results. Another method is the dynamic pressurization (DP) which keeps the specimen in a sealed vessel and suddenly increasing or decreasing pressure [24, 25]. By alternatively pressuring and depressuring, the effect of air voids in the unsaturated specimen can be gradually removed [25]. Indirect methods, requiring other data that can be used to calculate K_l , are referred as poromechanical (dynamic pressurization) techniques which monitor the time-dependent deformation of a specimen related to fluid flow in the pore network induced by externally applied stress or temperature change. The beam bending (BB) method is one such rapid indirect methods [26, 27, 28, 29] which was originally developed for soft gels and later was applied to cementitious materials. This method is based on the principle of exerting a certain strain to a long and slender specimen to obtain a relaxation curve, which is considered including both hydrodynamic and viscoelastic effects. By fitting this relaxation curve, K_l can be determined. This method has very clear requirements for the geometry of the specimen which makes it less applicable for concretes due to needing inconveniently large specimens to obtain a representative volume including aggregates. A method so-called thermopermeametry (TPA) was also introduced to cementitious materials on the basis of research

about gels [30, 31, 32, 33]. Given that the thermal expansion of liquid is always much greater than that of the solid phase, this method can determine K_l by measuring the rate of strain relaxation as liquid water flows out of the material after a temperature change.

Measurements of K_l are very sensitive to saturation conditions since the fully saturated condition is not easy to achieve. The presence of air voids or entrapped air in non-fully saturated materials may have a great influence on the measured results of the poromechanical methods and long delays in reaching equilibrium in conventional methods [34]. To ensure the fully saturated condition, various approaches were used in the literature, such as curing the specimen in water/limewater [23, 12], vacuum saturation [35] and pressurizing saturation [28, 29]. The time needed to fully saturate a porous body increases with the square of its smallest dimension. For the direct methods, the thickness of a disc specimen ranges from 25 to 70 mm (see the review in [19]) depending the size of aggregates as El-Dieb and Hooton [15] suggested that the specimen thickness should be 3 times as large as the aggregate size and a recent study [36] even reported that the specimen needs to be about 10 times as thick as the aggregates; therefore, a specimen may be extremely difficult to saturate. By contrast, the specimen in BB measurements is much easier to saturate since the method is limited to paste and mortar, so the diameter of the cylinder can be smaller than the concrete specimens used in the conventional methods.

In addition to experimental measurements, water permeability can be inferred by using information related to the microstructure, such as pore size distribution (PSD), porosity, tortuosity, connectivity, etc. A relationship was first proposed by Kozeny in 1927 [37] and later modified by Carman [38, 39] which is commonly known as the Kozeny–Carman (KC) equation. This equation was developed after considering a porous material as an assembly of capillary tubes for which the Navier–Stokes equation can be applied. It yielded K_l as a function of the porosity, the specific surface, and the shape and tortuosity of channels. It has been found that the KC equation is approximately valid for sands but not for clays [40]. Wong et al. [41] adopted a modified KC equation incorporating tortuosity and constrictivity to predict the oxygen permeability for concrete and they concluded that this equation overestimated the permeability by about one order of magnitude.

Based on mercury intrusion porosimetry (MIP) data for assessment of the percolation radius of the microstructure and resistivity measurements to determine the formation factor (inversely proportional to the product of porosity and tortuosity), the Katz-Thompson model [42] (KTI model) has proven useful for estimating the permeability of sedimentary rocks. Another version of this model avoids the use of resistivity measurements by assessing the formation factor only using mercury intrusion (KTII model) [43]. Baroghel-Bouny et al [44] showed that the KTI relationship slightly overestimates the permeability for concretes and mortars. The investigations of KTII performed by El-Dieb and Hooton [45] illustrated that this model leads to a more pronounced overestimation; the correlation can even be quite low for cementitious materials. Recent study by Zhou et al. [9] showed that KTII can provide similar results to measure nitrogen gas permeability with Klinkenberg correction, but it is about 2-4 orders of magnitudes higher than water permeability.

Other methods based on theoretical models are also reported in the literature. For instance, a practical method is to use measured sorptivity to assess K_l [12] because sorptivity measurements are much easier to perform than the above-mentioned permeability measurements. The first author of this paper introduced two methods to indirectly determine water permeability [8]. One is called “inverse analysis” that utilizes a numerical moisture transport model to back calculate K_l based on the measured drying mass loss curve. The other one employs the measured diffusivity curve to fit K_l by a general expression including both liquid transport and vapour diffusion.

As stated above, various methods using different specimen geometry or theoretical models in the

literature to determine K_l show that the reported permeability values have great dispersion, ranging from 10^{-22} to 10^{-17} m² for materials with the same water-to-cement ratio (see review in [8]). Even though researchers are apt to compare these values from different studies, K_l determined by various methods is not directly comparable, because:

- (1) the cements are different (the chemical composition of cements from different cement plants vary),
- (2) specimen preparation procedures are different (although the same preparation procedure is claimed in different studies, the variations of experimentalists, equipment, environment, etc, are unavoidable),
- (3) and specimens curing methods are different.

To eliminate these artificial effects, the present study employs a slender specimen for various methods to determine water permeability K_l . This long cylinder was initially prepared for the BB method. After the BB measurements, it was cut into several short cylinders and many slices. Some of short cylinders were used in sorptivity measurements and the others were used in drying experiments which provided the calibration data for a moisture transport model. Slices were used to measure the desorption isotherm which serves as the input data for the numerical model. Meanwhile, a small part of this slender cylinder was crushed to prepare specimens for MIP, nitrogen adsorption (NAD) and thermogravimetric analysis (TGA) tests.

The structure of this paper is given as follows. Firstly, a moisture transport model with K_l as the only undetermined parameter will be introduced, and then methods used to determine K_l will be briefly described. Experiments are carried out to obtain data for permeability determination methods and the moisture transport model. Finally, results from these methods will be compared and discussions on these methods will be presented.

2 Moisture transport model

2.1 Governing equations

Even though the multiphase model can be simplified as a single-phase model with liquid water [2], the authors also pointed out that this simplified approach is only suitable for the case of drying of low permeability materials with the initial condition close to saturation and exposed to a high relative humidity (RH) boundary condition. In that situation, liquid water governs mass transport [3, 46], while in a lower RH range vapour diffusion is non-negligible. The model selected here to simulate moisture transport in cementitious materials is the semi-simplified version of the multiphase model - including the transport of both liquid water and water vapour - which considers that gas pressure is constant and the liquid phase remains incompressible. The governing equation for the mass balance is written as [6, 7, 8]

$$\rho_l \frac{\partial S}{\partial t} = \frac{1}{\phi} \operatorname{div} (J_l + J_v) \quad (1)$$

where S is the degree of saturation, ρ_l (kg · m⁻³) is the density of liquid water, ϕ is the porosity of the porous material, and J_l and J_v (kg · m⁻² · s⁻¹) are the fluxes of liquid water and water vapor, respectively.

Liquid water transport consists of both contributions of capillary viscous movement of free water and the transport of physically-adsorbed water molecules in a single Darcy relation in which capillary

pressure and relative permeability are derived from the sorption curves over the whole range of RH through the liquid water saturation S (-). Moreover, the viscosity of pure water is used for both free water and bound water. The driving force for liquid transport is the gradient of liquid pressure P_l (Pa) [2, 6]:

$$J_l = -\rho_l \frac{K_l k_{rl}(S)}{\eta} \mathbf{grad} P_l \quad (2)$$

where η (Pa · s) represents the dynamic viscosity of liquid water, and k_{rl} (-) is the relative liquid permeability which is generally treated as a function of S .

The flux of vapor J_v is described as a diffusion-like process with the vapor density ρ_v (kg · m⁻³) as the main variable [2, 3].

$$J_v = -D_{v0} f(S, \phi) \mathbf{grad} \rho_v \quad (3)$$

where D_{v0} (m² · s⁻¹) is the free vapor diffusion coefficient in the air. The parameter $f(S, \phi)$ represents the resistance factor for gaseous diffusion and is related to the connectivity and tortuosity of the pore network.

In this moisture transport model, the thermodynamic equilibrium between the liquid and vapor is assumed. The equilibrium state is governed by Kelvin's law which is written in the following form:

$$P_c = -\frac{\rho_l R T}{M_v} \ln \text{RH} \quad (4)$$

where $R = 8.314 \text{ J} \cdot \text{K}^{-1} \cdot \text{mol}^{-1}$ is the gas constant, T (K) is the absolute temperature and M_v (kg · mol⁻¹) is the molar mass of water molecule. Capillary pressure in the macroscopic scale is defined as the difference between gas pressure and the liquid phase pressure ($P_c = P_g - P_l$). The relationship of P_c as a function of S is known as the capillary pressure curve. For cementitious materials, this curve is indirectly measured by means of sorption experiments performed at constant temperature (so-called water vapor sorption isotherms) [47]. Various equations can be found in the literature to describe sorption isotherms [48]. One well-known equation was proposed by van Genuchten (VG equation) [49],

$$P_c(S) = \alpha (S^{-1/m} - 1)^{1-m} \quad (5)$$

where α (Pa) and m are two fitting parameters.

The flux boundary condition (also known as convective condition [50]) is used to account for an imperfect moisture transport between the environment and the surface of the material. The expression is given as [35]

$$q = (J_l + J_v)_{x=0} = \phi S_0 E (P_v^0 - P_v^e) \quad (6)$$

This boundary condition includes a material property (porosity ϕ), a parameter related to the environment (external vapor pressure P_v^e), the moisture state within the material near the surface (P_v^0 and its related liquid-water saturation S_0) and the interaction between the ambient environment and the material (through the emissivity E). The term ϕS_0 takes into account the reduction of wet surface when exposed to the environment. The emissivity E (kg · m⁻² · s⁻¹ · Pa⁻¹) has been assessed from experiments which proposed a value around $2.58 \times 10^{-8} \text{ kg} \cdot \text{m}^{-2} \cdot \text{s}^{-1} \cdot \text{Pa}^{-1}$ [51, 35] for a laboratory environment where RH and temperature are maintained constant (atmospheric

pressure, $RH = 50 \pm 5\%$ and $T = 293\text{ K}$).

Putting Eqs. (2) - (5) back into the mass balance equation, Eq. (1), and combining the initial and boundary conditions (see Eq. 6), the moisture transport problem can be solved.

2.2 Transport coefficients

The resistance factor in Eq. (3) represents the reduction of accessibility for water vapor diffusion which is due to the presence of the solid and liquid phases, the tortuous path for diffusion, the different connectivities in the pore network, etc. Because of limited experimental results, the expression of $f(S, \phi)$ is generally derived from theoretical concepts. For example, Millington and Quirk [52] deduced an equation for granular materials (soils):

$$f(S, \phi) = \phi^{x_D} (1 - S)^{x_D+2} \quad (7)$$

Millington and Quirk [52] proposed that parameter x_D was fixed at $4/3$. However, granular materials are more porous than cementitious materials, so resistance to water-vapor diffusion may be more significant for cementitious materials. Thiéry et al. [53] suggested $x_D = 2.74$ based on the fitting of experimental data for cement pastes and mortars taken from Papadakis et al. [54]. The comparison of $f(S, \phi)$ calculated by these two proposed values of x_D shows that Thiéry's suggestion provides smaller $f(S, \phi)$ values (higher resistance) which may be closer to the real conditions of cementitious materials than the original x_D value for granular materials [8].

Another important transport coefficient is the relative permeability k_{rl} . For cementitious materials, measuring the permeability to liquid-water for different RH is very difficult due to the fact that advective liquid transport and vapor diffusion always occur together; therefore, measured results include both transport mechanisms [6]. Owing to these reasons, it is acceptable to assume that k_{rl} is a unique function of S . One well-known model is the van Genuchten – Mualem equation (VGM) which was first reported by van Genuchten [49]. It is formulated as a simple analytical relation

$$k_{rl}(S) = S^\ell \left[1 - (1 - S^{1/m})^m \right]^2 \quad (8)$$

In Eq. (8), m is the same as in Eq. (5). The term S^ℓ is a correction factor which accounts for the influence of tortuosity. Different suggestions of parameter ℓ have been proposed by researchers [55, 56]. In Mualem's research, ℓ varies between -1 and 3, and the value 0.5 was considered as the best choice. This value has also been used for cementitious materials [2, 57].

3 Determination of liquid permeability

Methods chosen here for the determination of K_l are primarily based on whether these methods can share the same specimen and whether this specimen can be used to obtain input and calibration data for the moisture transport model. The pivotal factor is the geometry of the specimen for these experimental methods. The KC and KTH equations need the crushed specimens to measure PSD, so they do not require a geometry for preparing specimens, and the same is true of the desorption isotherm measurements which only need small pieces. The ideal geometry for the drying experiments and the sorptivity measurements is a cylinder which is also convenient for performing 1D simulations. Owing to the large specimen size in the traditional flow-through methods, they suffer from the fact that the specimen can not easily be fully saturated. Considering the availability

of equipment as well, we finally selected the following methods to determine K_l : beam bending, sorptivity, KC and KTII equations.

3.1 Beam bending

Three-point beam bending has been developed as a method to measure the liquid permeability of a porous body [26, 27, 28, 29]. This method can provide permeability results within a few minutes to a few hours, whereas conventional techniques often require days and weeks. When a saturated porous material is bent, pressure gradients are created in the liquid, which flows within the pores to equilibrate the pressure. This phenomenon can be exploited to measure permeability, because a poroelastic analysis indicates the expected rate of change of the force $W(t)$ needed to sustain a constant deflection of the beam as the pore pressure relaxes [26]; by comparing the measured relaxation kinetics to the theoretical curve, the permeability K_l can be extracted.

When a saturated porous rod is subjected to bending, the flow in the porous medium is assumed to obey Darcy's law. The hydrodynamic relaxation is the process by which the liquid flow reestablishes ambient pressure throughout the specimen. The relaxation function $R(t)$ is given by normalizing the force exerted on the specimen $W(t)$ by the initial force $W(0)$.

$$R(t) = \frac{W(t)}{W(0)} = 1 - A + AS_r(t) \quad (9)$$

where the constant A is

$$A = \frac{\left(\frac{1 - 2\nu_p}{3}\right) \left(1 - \frac{B_p}{B_s}\right)^2}{1 - \frac{B_p}{B_s} + (1 - \phi) \left(\frac{B_p}{B_l} - \frac{B_p}{B_s}\right)} \quad (10)$$

where $B = E(3(1 - 2\nu))$ is the bulk modulus. ν is the Poisson's ratio which is taken as 0.2 for cementitious materials [28, 29]. Subscripts p , l and s represent properties of porous body, liquid phase and solid phase, respectively. For a cylindrical specimen, the relaxation function can be approximated as

$$S_r(t) = \exp \left[-\frac{8}{\pi^{1/2}} \left(\frac{\theta^{1/2} - \theta^{5/2}}{1 - \theta^{1/2}} \right) \right] \quad (11)$$

where the reduced time is defined as

$$\theta = \frac{t}{\tau_R} \quad (12)$$

where the hydrodynamic relaxation time τ_R is defined as (with the approximation $B_p/B_s \approx \phi^2$ for cement pastes [28])

$$\tau_R = \left[\frac{2(1 + \nu_p)}{3B_p} + \frac{1 - \phi}{B_l} - \frac{1}{B_s} \left(\frac{\phi^2 - 5\phi + 8}{5} \right) \right] \left(\frac{\eta r^2}{K_l} \right) \quad (13)$$

where r (m) is the radius of the cylindrical rod.

In the experiments, a constant displacement δ is suddenly applied to the rod within the linear elastic range and the force decay over time is continuously measured. The measured curve is then

fitted by Eq. (9) with A and τ_R as free parameters. From the plateau of the force relaxation curve, Young's modulus of the porous body can be calculated.

$$E_p = \frac{L^3(1-A)W(0)}{12\pi r^4 \delta} \quad (14)$$

where L (m) is the support span.

According to the analytical solution for viscoelastic materials in [26], the total relaxation of the slender specimen is the product of the hydrodynamic $R(t)$ and the viscoelastic $\Psi_V(t)$ relaxation functions.

$$\frac{W(t)}{W(0)} = R(t)\Psi_V(t) \quad (15)$$

This equation is valid for cases that the viscoelastic relaxation time τ_V is an order of magnitude longer than hydrodynamic relaxation time τ_R . For a short-term measurement (e.g., a few hours), the viscoelastic relaxation function can be formulated by an exponential function.

$$\Psi_V(t) = \exp \left[- \left(\frac{t}{\tau_V} \right)^{b_V} \right] \quad (16)$$

where $b_V \subseteq [0, 1]$ is a constant. The properties of liquid are taken from paper [28]; thus, the fitting parameters can be determined and then used to extract K_l .

3.2 Sorptivity method

Sorptivity is defined as “a measure of the capacity of the medium to absorb liquid by capillarity” [58]. It can be easily measured by simple experiments. Considering that the initial stage of mass changes in an absorption test is mostly controlled by capillary suction, sorptivity S_p (m/s^{1/2}) can be determined by the cumulative volume of water crossing the specimen surface [59]

$$\frac{\Delta m}{A_r \rho_l} = S_p t^{1/2} + a \quad (17)$$

where Δm (g) is the measured mass change of the specimen, A_r (m²) is the area of the specimen's cross-section, and a is a parameter associated with the end effect (such as buoyancy, lateral invasion). Using sorptivity directly to determine permeability is rarely discussed in the literature. Nevertheless, the determination of water diffusivity from sorptivity has been studied for several decades [60, 61, 62]. The relation between water diffusivity D_l and permeability K_l is

$$K_l = D_{l0} \mu \theta_s \left. \frac{dS_l}{dP_l} \right|_{S_l=1} \quad (18)$$

where D_{l0} (m²/s) and $\theta_s \left. \frac{dS_l}{dP_l} \right|_{S_l=1}$ are water diffusivity and water capacity of the porous material at saturated condition ($S_l = 1$), respectively, and $g=9.81$ m/s² is the gravitational acceleration. For cementitious materials, Zhou [63, 12] proposed the following equation for D_{l0}

$$D_{l0} = \tau_D \exp(n) \left(\frac{S_p(\theta_i)}{\theta_s - \theta_i} \right)^2 \quad (19)$$

where θ_s and θ_i are saturated and initial water contents, respectively, and n is a shape parameter related to the initial saturation $S_{l,0}$ and can be expressed as $n = n_0(1 - S_{l,0})$ (n_0 is the shape parameter for initially dried specimen). The coefficient τ_D can be either fitted by experimental data or calculated by [64]

$$\tau_D = \frac{n^2}{(2n - 1) \exp(n) - n + 1} \quad (20)$$

The water capacity $\theta_s \frac{dS_l}{dP_l}$ is generally calculated from the sorption isotherm, while most isotherm equations show that the water capacity at saturated condition is infinity (e.g., Eq. (5)) or zero, which leads to meaningless K_l in Eq. (18). Zhou [65] proposed a new equation for sorption isotherms.

$$S_l = \left[1 - c_1 + c_1 \exp\left(\frac{P_c}{c_2}\right) \right]^{-1} \quad (21)$$

where c_1 and c_2 (Pa) are two fitting parameters. Thus, $\frac{dS_l}{dP_l}$ is the derivative of this function at $S_l = 1$.

$$\left. \frac{dS_l}{dP_l} \right|_{S_l=1} = \frac{c_1}{c_2} \quad (22)$$

Putting Eqs. (19) and (22) back to Eq. (18), K_l can be calculated by the measured sorptivity S_p .

3.3 Katz–Thompson (KT) equations

Many attempts have been made to link the transport properties of porous media and their microstructure. One of the theories that have been widely used is Katz-Thompson (KT) theory which was initially developed to predict the permeability of sedimentary rocks. The percolation theory was employed in KT relation, that introduces the characteristic length as one of main inputs (KTI) [42].

$$K_l = \frac{d_c^2}{226} \left(\frac{\sigma}{\sigma_0} \right) \quad (23)$$

where d_c is the characteristic dimension of pore space, which corresponds to the peak in the derivative of PSD, σ is the electrical conductivity of the saturated porous material and σ_0 is the conductivity of pore solution. The coefficient $1/226$ is used for general porous materials, but for concrete different values were suggested (e.g., $1/8$ for the lightweight concrete [66]). In this study, the modified values are not used because $1/226$ is an analytical constant by assuming cylindrical pores in the MIP measurements [67], so it should not vary with materials. The conductivity was used to reflect the tortuosity of the pore network but it must be measured separately. Katz and Thompson [43] proposed an expression for the conductivity term (σ/σ_0) which can be estimated from MIP data (KTII).

$$\frac{\sigma}{\sigma_0} = \frac{d_{max}^e}{d_c} \phi V(d_{max}^e) \quad (24)$$

where d_{max}^e is the electrical conductivity characteristic dimension that produces the maximum conductance. For a very broad PSD, d_{max}^e is estimated by $d_{max}^e = 0.34d_c$ [43]. $V(d_{max}^e)$ is the fractional volume of connected pore space with pore size larger than d_{max}^e . d_c is normally taken as the critical

(or breakthrough) pore diameter, representing the minimum radius which is geometrically continuous throughout hydrated cement paste.

By using Eq. (24), without adjusting parameters, Katz and Thompson concluded that permeability and σ/σ_0 can be predicted from the same MIP data [43]. They found that the calculated σ/σ_0 showed good agreement with the directly measured values for sedimentary rocks.

3.4 Kozeny–Carman (KC) equation

Considering that the flow in one-size straight tubes obeys Navier–Stokes (N-S) equation, Hagen–Poiseuille equation is an exact solution to the N-S equation. Meanwhile, Darcy’s law can give the flux through these tubes. The comparison of Hagen–Poiseuille equation with Darcy’s law yields water permeability K_l as a function of the porosity ϕ , the specific surface S (m^2/kg), and tortuosity of channels τ . One widely used version was proposed by Walsh and Brace [68].

$$K_l = \frac{\phi^3}{2\tau^2 S^2 \rho_s^2} \quad (25)$$

where ρ_s (kg/m^3) is the bulk density of the dried material. As stated above, Eq. (25) is developed for tubes having the same cross-sections. To account for the various sizes of pores, an equation adapted by Walsh and Brace [68] can be used here.

$$\frac{\phi}{\tau^2} = \frac{\sigma}{\sigma_0} \quad (26)$$

where the term σ/σ_0 is formulated in Eq. (24). A similar equation for cementitious materials was also proposed by Wong et al. [41] who introduced a constrictivity factor and proposed a modified equation for permeability, but they found that the equation largely overestimated permeability. By plugging Eq. (26) into Eq. (25), we thus have the version of KC equation that will be used in this study.

$$K_l = \frac{\phi^2}{2S^2 \rho_s^2} \left(\frac{\sigma}{\sigma_0} \right) \quad (27)$$

Since the tortuosity and porosity factors are included in this equation, it is supposedly representative of the pore structure in a porous material.

4 Experiments

Measurements can be affected by many factors, such the type of cement, mixture procedure, the size of specimens, curing condition, etc. To avoid these artificial factors, we prepared all specimens in one batch. For most measurements (beam bending, sorption isotherm, drying, MIP, sorptivity), specimens are obtained from the same cylinder to minimize the influence of batch differences. The cement used in this study was a Type I ordinary Portland cement (OPC) from Buzzi Unicem, USA. Chemical and mineralogical data were given in [69].

The specimen preparation basically followed the procedure reported in [28]. The cement paste with water-to-ratio of 0.5 is used in this study. After adding deionized water into cement powder, the material was hand mixed for 1 minute and then mixed by a vortex mixer (Stuart Vortex Mixers SA8) for additional 3 min. Before casting paste in the polystyrene pipettes, which were lubricated

by petroleum jelly, the fresh paste was deaired for about 4 min. Two sizes of cylindrical specimens were prepared, 8 and 16 mm in diameter. After 48 h curing, cylinders were removed from the pipettes, wiped with lab tissues, and stored in limewater for further curing.

4.1 Measurements for K_l methods

4.1.1 Beam bending

After one year, both 8 and 16 mm-diameter specimens were subjected to the beam bending measurements. Specimens were taken out and pressurized in a limewater-filled tube for one day to ensure that specimens were fully saturated prior to the tests. The test procedure has been well illustrated in the literature [28, 29, 70] and a brief introduction is given here. The pushrod, which directly touched the slender specimen during tests, was controlled by a stepper motor to apply the sudden displacement. A linear-variable differential transformer (LVDT) was used to measure the deflection. A 250 g load cell was used to measure the load force. Since the relaxation is most rapid in the beginning, the data were recorded at logarithmic time intervals. The slender specimen was placed in a stainless steel container which was filled with limewater. Two V-shape steel supports were used to ensure good alignment of the cylindrical specimen and to avoid any movement during tests. The assembly was placed in an incubator to maintain constant temperature. The displacement applied depends on the radii of the specimen r and the support span L . To have accurate results, the span L must be longer than ten times the specimen diameter ($L > 20r$).

4.1.2 Sorptivity

After BB tests, one of the 16 mm-diameter cylindrical specimens without any defects (mainly air voids, which can only be checked after cutting) was used to prepare specimens for other measurements. About 5 mm from each end of the cylinder was removed and discarded. The remaining part was gently cut by a diamond saw into many slices (about 1 mm thick) and several 20 mm long cylinders. Some short cylinders were used for the measurement of sorptivity. These cylinders were preconditioned for three months in cups with constant RHs (97%, 85%, 63% and 53%) which were achieved by using saturated salt solutions (see Table 1 for details). In the sorptivity measurements, only one end of the short cylinder can contact water. To minimize moisture exchange between the specimen and its surroundings, the side of the cylinder was sealed with the adhesive aluminum sheet and the other end was loosely covered to let gas escape when water penetrates from the opposite end. About 1 mm of the side surface at the end that contacts water was not sealed by the aluminum sheet. This can avoid the aluminum sheet contacting water and creating errors during measurements. An electronic balance (Denver Instrument) with accuracy ± 0.001 g was connected with a data acquisition system (DAQ) to automatically record the mass change (see Fig. 1 for details). The top of the balance was covered to eliminate the air flow effect in the lab. A screwed fixture under the balance was used to grasp the specimen. Data recording every second started just after the specimen was fixed. A beaker with water was seated on a small lift that can be manually elevated until water just touches the bottom end of the specimen. The beaker was large enough (about 30 cm in diameter) to ensure that the drop of water level during measurements can be neglected. The beaker was covered by the plastic film and only a hole in the center was left for the specimen to pass through. Because the ambient RH is different to RHs for preconditioning, the time between taking the specimen out the cup and the beginning of the test should be as short

as possible. Data logging continuously ran about 20 h but only the measured mass change curve at the initial stage was used to calculate sorptivity.

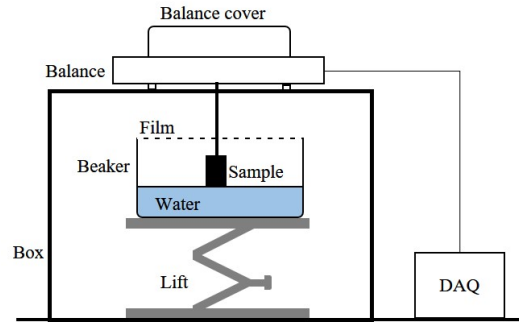


Figure 1: Illustration for sorptivity measurements.

4.1.3 MIP, NAD and TGA

A small part of the slender specimen was used to prepare specimens for MIP, NAD and TGA measurements. As reported in our previous studies, different drying methods have significant effects on the microstructure [71, 69], so two drying methods were compared in this study: oven drying at 60°C while flushing with N₂ and isopropanol (IPA) replacement followed by drying under flowing N₂ at room temperature. The details of these two drying methods can be found in [69]. Part of the rod was crushed into lumps (about 3 mm) which were subjected to different drying methods and fine powders were used for the first TGA test (labelled with “No drying”). After drying, lumps were further crushed and sieved. Particles with size < 0.6 mm were used for the TGA measurements, size between 0.6 and 1.2 mm were used for the NAD tests and size about 3 mm were used for the MIP measurements. TGA measurements were performed by PerkinElmer[®] Pyris 1, in which specimens were heated from room temperature to 1000 °C. The measured mass change between 105 °C and 1000 °C was used to calculate the degree of hydration (DoH). The detailed procedure and equation were reported in our previous studies [72, 71, 69]. The NAD measurements were conducted using an ASAP 2010 apparatus, from Micromeritics (see [71] for more details). The Micromeritics 9410 apparatus was used for MIP tests (see [73] for details).

4.2 Measurements for moisture transport model

4.2.1 Sorption isotherm

The desorption isotherm was measured by using saturated salt solutions to establish ten different RHs (see Table 1). At each RH, three thin slices (initially saturated) with thickness around 1 mm, which were cut from the 16 mm-diameter cylindrical specimen, were used to determine the water content. There was about 50 ml saturated salt solution in a 200 ml cup and a plastic mesh was installed in the middle that specimens were placed on. There was a small hole in the lid of the cup, so that the hang wire could pass through and the lower end was hooked to a specimen pan containing one slice. A rubber stopper was used to seal the hole in the lid between measurements. When measuring the mass of the slice, one just needs to remove the rubber stopper and connect the upper end of the hang wire with the electronic balance. Thus, the mass change of the specimen

could be regularly monitored with minimal disturbance caused by opening the cup. Note that water content at different RHs was measured by using different specimens, this can greatly reduce measuring time compared with the stepwise method for the same specimen (e.g., [47]).

Table 1: Salts used to control different RHs.

RH %	11	22	33	44	53	63	75	85	92	97
Salt	Lithium	Potassium	Magnesium	Potassium	Magnesium	Sodium	Sodium	Potassium	Potassium	Potassium
	Chlo-	Ac-	Chlo-	Carbon-	Ni-	Bro-	Chlo-	Chlo-	Ni-	Sulfate
	ride	etate	ride	ate	trate	mide	ride	ride	trate	
Formula	LiCl	KCH ₃ COO	MgCl ₂	K ₂ CO ₃	Mg(NO ₃) ₂	NaBr	NaCl	KCl	KNO ₃	K ₂ SO ₄

4.2.2 Drying tests

Drying tests at RH = 22, 53, and 63 % were performed on the short cylindrical specimens that were first preconditioned at RH=97% rather than starting from the saturated condition. The preconditioning was done by putting the initially saturated short cylinders in a cup with 97% RH and keeping at 40 °C for about three days. The cup was then moved to the room temperature for one month. The high temperature used here can speed up water evaporation and reduce preconditioning time. After preconditioning, it was assumed that moisture uniformly distributed in the specimen. The cylinders were then sealed by the adhesive aluminum sheet on the side and only two ends were exposed to the corresponding RH environment. The cups with the same design as the desorption isotherm measurements were used for drying tests. The masses of these specimens were regularly weighted for about three months.

After tests, some short cylinders (from sorptivity measurements and drying tests) were dried in an oven at 60 °C to obtain the mass at dryness. Since the geometry of these cylinders were well defined, the mass difference between the dried and saturated states can be used to determine the porosity.

5 Results

5.1 K_l determined by different methods

Specimens with two diameters (8 and 16 mm) were used in the beam bending tests and one example for the larger specimen is shown in Fig. 2. Good agreement between measured and fitted relaxation curves can be seen in this figure with well separated hydrodynamic and viscoelastic relaxation curves. The inflection point represents the end of the hydrodynamic relaxation and is clearly shown at about 1000 s. This time is much delayed compared with those reported in [28, 29] because the material in the present study is older. Consequently, the measured permeability (shown in Table 2) is lower than those in [28, 29].

Table 2 shows data form the BB tests for two specimens. If the flow is radial, Eq. (13) indicates that the hydrodynamic relaxation time depends on the square of the radius. As shown in Table 2, τ_r for the 16-mm specimen is about 4 times the average τ_r for 8-mm specimen^a. This means that the results scaled with the specimen size are in agreement with the theory.

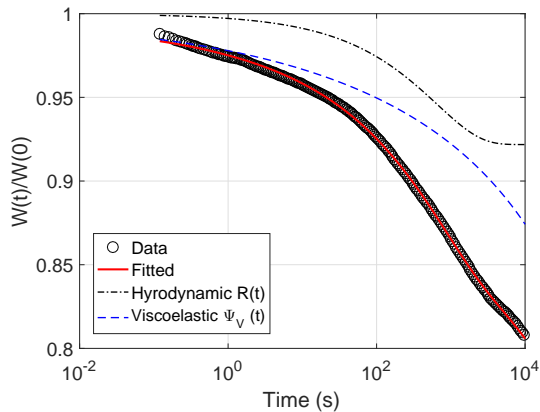


Figure 2: Measured and fitted relaxation curves for BB tests ($2r=16$ mm).

Table 2: Parameters in the beam bending method for different size of specimens.

Specimen diameter	E_p (GPa) ^b	τ_R (s)	K_l (10^{-21}m^2)
16 mm	23	20410	0.679
8 mm(1st)	23	8469	0.4
8 mm(2nd)	23	2189	1.4

Even though the sorptivity tests ran about 20 h, after a certain period (about 10 h in this study), the rate of mass increase started to drop because the water penetration front reached the top of the specimen. At the initial stage, water uptake is supposed to be a nearly linear function of the square root of time as indicated in Eq. (17). In this study, we only took the linear part of the measured curves to fit sorptivities for specimens with various initial water contents. Fitted and measured results are compared in Fig. 3 showing very good fittings.

The fitted sorptivities for all tests are given in Table 3 which clearly shows the decrease of S_p with the increase of the initial water content. This is very reasonable when the specimen has less water in the pore network (large pores are not filled with liquid water), the initial capillarity is much stronger than specimens having more water inside, and thus water uptake is much faster at the initial stage. The parameter n_0 in Eq. (19) is a material-dependent parameter. Since only one material is studied here, we take $n_0 = 6$ for all tests [64]. Note that this value is smaller than those in [12] ($6.2 \sim 7.6$) for concretes. The calculated permeabilities based on measured sorptivities in Table 3 show a very small variation with all values in the same order of magnitude.

A clear tendency is seen for initial RH from 53 - 85 % as the calculated K_l decreases due to the decrease of sorptivity. Nevertheless, K_l for initial RH = 97% is much higher these for the other initial RHs. The primary reason is that 97 % RH only can remove water in the large capillary pores

^aIt generally plots the τ_R vs. r^2 curve, which shows that two tests for 8 mm specimens scatter around a line that passes through the origin, but the average value of τ_R is on the same line with the 16 mm specimen.

^bThe Young's modulus is taken from [74] which reported 22.8 ± 0.5 GPa for the mature cement paste. In fact, the value of E_p does not affect the calculated permeability which is mainly dependent on the inflection point of the measured force relaxation curve. τ_R is the parameter controlling the position of the inflection point. For cementitious materials, in which B_p and $B_s \gg B_l$ [75], Eq. (13) can be approximately replaced by $\tau_R \approx \left(\frac{1-\phi}{B_l}\right) \left(\frac{\eta r^2}{K_l}\right)$. It is clear that K_l is primarily dependent on the mechanical property of liquid.

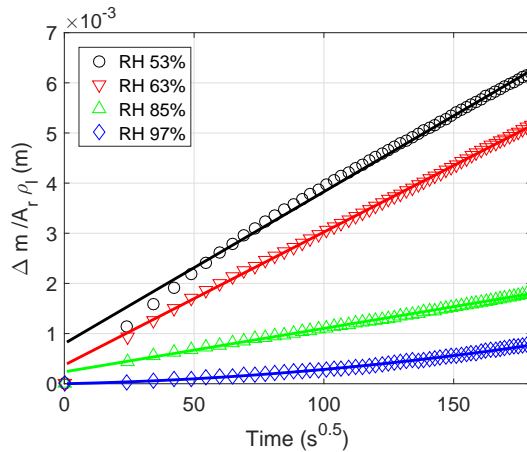


Figure 3: Measured and fitted sorptivity experimental curves (symbols are measured and lines are fitted). The number of measured data is reduced to clarify.

(> 35 nm according to Young-Laplace and Kelvin equations), so the small capillary and gel pores are not affected under this drying condition. Theoretically, water transport in all pores should be included in the measurements; this is, a completely dried specimen is more representative than a partially dried specimen, while drying can change the virgin microstructure. The compromise between drying condition and microstructural change must be well analyzed prior to performing sorptivity measurements. In addition, we found that K_l for initial 97 % RH is very sensitive to the choice of sorption isotherms. For instance, K_l determined by using the measured saturation is about 2 times greater than that by using saturation calculated by the VG equation. Therefore, results presented in Table 3 use the measured sorption data. This also implies that the use of specimens with high initial water content is inappropriate for the sorptivity method.

Table 3: Results from sorptivity tests.

RH (%)	53	63	85	97
S_p ($10^{-5}\text{m}/\text{s}^{0.5}$)	3.03	2.56	0.866	0.108
K_l (10^{-21}m^2) ^c	165	153	104	503

Results from MIP, NAD and TGA are provided in Table 4 for specimens dried by different methods. After one year hydration, about 11% cement is still unhydrated, which is largely due to the fact that the cores of some cement grains have less accessibility to water because of the shell around them and the complex pore network in cementitious materials. The specimen dried by N_2 at 60 °C shows a slight lower DoH than the undried specimen. This is because 60 °C leads to the decomposition of some hydration products (mainly ettringite) and the loss of chemically bond water [71]. The isopropanol replacement shows higher DoH than others. This difference could be attributed to stronger interactions of IPA (probably strong physical adsorption) with hydration products (mainly calcium hydroxide), so that IPA is gradually released during heating in the TGA [71]. Drying effects are also clearly shown in the surface area measured either by N_2 BET or by MIP. They

^cSaturation and water content in Eq. (19) are taken from the measured sorption isotherm rather than calculated by the VG or Zhou's equations.

both show that IPA replacement provides higher surface area than nitrogen drying at 60 °C. It is generally believed that IPA replacement preserves the fine microstructure, while the capillary force induced by water evaporation during the flowing nitrogen drying can cause the collapse of the fine microstructure. In addition, the N₂ BET surface area is always higher than MIP as reported in the literature [76]. This results from the fact that mercury is not able to enter the fine pores that need high intrusion pressure which may damage the fine pore structure. This difference is also illustrated by the porosity measured by the mass difference and MIP in Table 4.

The permeability values in Table 4 are calculated based on MIP data. NAD data are not used here because the calculated incremental PSD monotonically increases with the pore size and therefore the critical pore diameter can not be identified. K_l provided by the KC equation is about three times as low as that by KT equation for both drying methods. The version of KT equation used in this study (KTII, see Eq. (24)) is much simplified compared to the original one (KTI in [42]). KTII mainly relies on the measured critical pore size d_c and therefore the accuracy and robustness of KTII are also lower. The modified KC equation, by contrast, including the effects of surface area and density of solids, may be more representative for porous properties of a material.

Table 4: Results from MIP, NAD and TGA, and calculated K_l by KC and KT methods.

Specimen	DoH	$S(N_2)$ BET (m ² /g)	$S(MIP)$ (m ² /g)	d_c (μm)	ϕ	ρ_s^f (g/ml)	$K_l(KC)$ (10 ⁻²¹ m ²)	$K_l(KT)$ (10 ⁻²¹ m ²)
No Drying	0.886	-	-	-	0.358 ^d	-	-	-
N ₂ 60°C	0.842	108	57.4	0.05	0.250 ^e	1.569	81.2	233
IPA replace- ment	0.899	124	64.7	0.04	0.244 ^e	1.602	50.7	134

It is clear that these K_l values determined by various methods show a large scatter even though all tests were based on exactly the same material. The permeability K_l determined by the BB method is much lower than other methods. One possible reason is that the specimen used in the BB method is fully saturated and specimens are dried to some extent in the other methods. As reported in the literature [77, 71], any drying can alter the morphology of C-S-H gel and the microstructure of material to a certain degree. From this point, we expect that the BB method is able to provide K_l much closer to the “true” one than the other methods. The permeabilities from KT and sorptivity methods are very close and higher than KC. The reason for the difference between the sorptivity method and the others is unknown to us, and more work needs to be done for the sorptivity method since the microstructural changes during water absorption in cementitious materials are not considered by the sorptivity method.

5.2 Comparison of K_l from different methods

Measured and fitted desorption isotherms by Eqs. (5) and (21) are shown in Fig. 4. Fitted parameters for Eqs. (5) and (21) are provided in Table 5. The calculated adjusted determination coefficient R_{adj}^2 (equation can be found in [48, 46]) are very close to 1, indicating that both equations have a good applicability for the studied cementitious material.

^dMeasured by the mass difference of a specimen between saturated and dried (60°C) states.

^eMeasured by MIP.

^fCalculated based on MIP data.

Table 5: Fitted parameters for the measured desorption isotherm.

Equation	VG (Eq. (5))		Zhou(Eq. (21))	
Parameter	α (Pa)	m	c_1 (Pa)	c_2
	4.39E7	0.423	2.66E8	1.964
R_{adj}^2	0.994		0.992	

In Fig. 4, the VG equation shows slightly better fitting at high RH, while Zhou’s equation is slightly better at low RH.

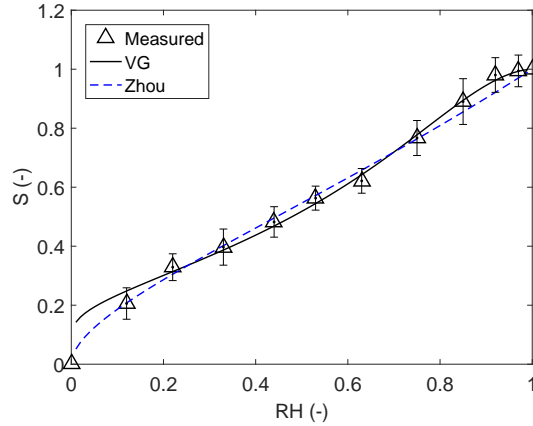
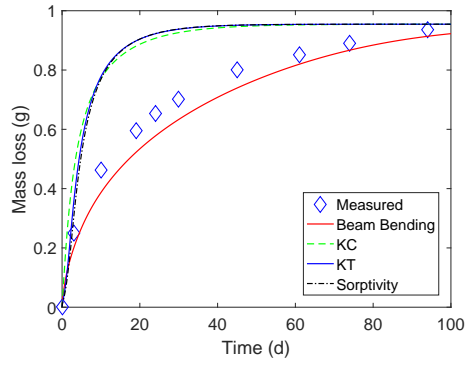


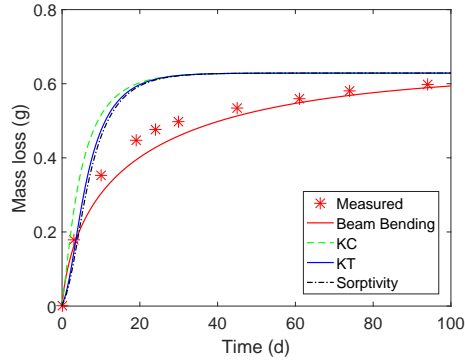
Figure 4: Measured and fitted desorption isotherm.

In the moisture transport model introduced in Section 2, K_l is the only unknown, so values calculated by the above methods can be used. By comparing the simulated mass loss curves using these K_l values with the measured ones, we can tell which K_l determination method is suitable for this moisture transport model. For the BB method, K_l measured for the 16-mm specimen is used for simulation since the drying tests were done for the specimens with the same size. For KC and KTII equations, K_l determined by the specimen dried by IPA replacement is chosen because we have shown that IPA replacement can better preserve the delicate microstructure of cementitious materials than the flowing nitrogen drying. For the sorptivity method, K_l values determined from specimens preconditioned at RH = 53 and 63% are directly used for drying tests with the corresponding RHs. For drying at RH = 22%, there is no corresponding sorptivity measurement, so we take the K_l value of the sorptivity measurement for initial RH = 53% ($1.65 \times 10^{-19} \text{ m}^2$).

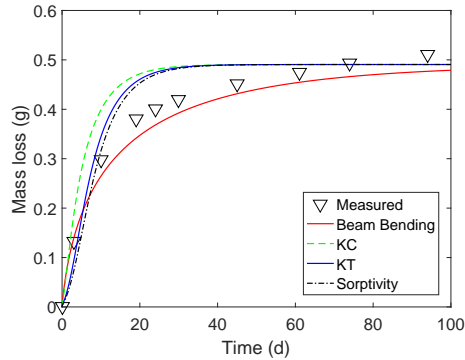
Comparison of measured and simulated mass loss curves in Fig. 5 clearly demonstrates that K_l determined by the BB method is able to provide the curves closest to the measured ones regardless of the drying condition. Although permeabilities by KC, KTII and sorptivity methods are different, the mass loss curves calculated by them are very close, because these permeabilities are so high that they cause mass loss quickly reaching the plateau. Therefore, the similar conclusion as the literature can be drawn that KC and KTII equations overestimate K_l by 1-2 orders of magnitudes [44, 45, 9]



(a) Drying test at RH=22%.



(b) Drying test at RH=53%.



(c) Drying test at RH=63%.

Figure 5: Comparison of measured and simulated mass loss curves.

6 Discussion

6.1 Inverse analysis

In fact, K_l in the moisture transport model can be determined by back calculation from the measured mass loss curve at a constant RH. This method was known as “inverse analysis” in the previous studies [78, 2, 79, 7, 8]. As discussed in [7, 8], the initial moisture state of calculations corresponds to the state after self-desiccation which is about the same RH used in this study for the preparation of specimens for drying tests. The previous study reported that the inversely determined K_l for the same material dried at two RHs is very close [7], which proves that the moisture transport model used

here is able to provide the consistent results for K_l . Moreover, water saturation profiles simulated by this moisture transport model match the measured ones very well. This further strengthens our confidence in using the moisture transport model in Section 2 for inverse calculation of K_l .

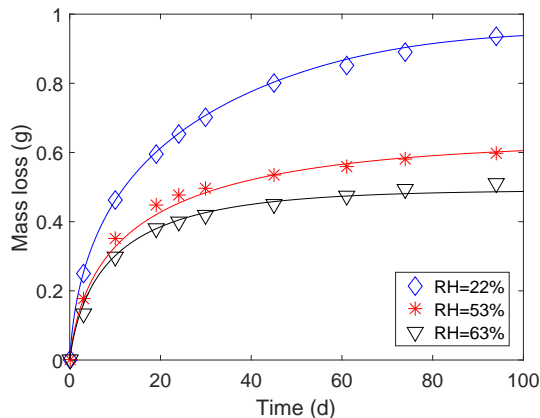


Figure 6: Comparison of measured and simulated mass loss curves for drying at three different RHs.

The fitted mass loss curves for drying at three different RHs are shown in Fig. 6. By only adjusting K_l in the moisture transport model (of course boundary condition must be changed to the corresponding drying condition), we are able to obtain very good fitting with the measured curves. Permeabilities inversely determined by fitting the measured mass loss curves are given in Table 6. The values of K_l for three different drying conditions are very close with difference less than a factor of two. Compared with permeabilities determined by the above methods, the inverse analysis shows K_l values much lower than those from KC, KTII and sorptivity methods and slightly higher than that from the BB method. This confirms our hypothesis that the BB method, using the saturated specimen, is able to provide K_l suitable for the moisture transport model employed here. As mentioned above, the good capability of the BB method is because the saturated specimen retains the original microstructure of cementitious materials while the microstructure of dried specimens in other methods is altered. There is no correction for the microstructural change in the KC and KTII equations. In the sorptivity method, the correction may be partially considered in the measured desorption isotherm. Nevertheless, during water absorption, the C-S-H gels undergo swelling, recovery and rearrangement [80, 81, 9], which are not taken into account in the sorptivity method. For the moisture transport model, the microstructural change is not directly considered by any equation, while the input data - the measured desorption isotherm - actually includes this information. Unlike the sorptivity method, the inverse analysis is not affected by the wetting of C-S-H gels.

Table 6: Permeabilities determined by the inverse analysis.

Drying	RH	22	53	63
(%)				
K_l (10^{-21} m ²)		2.2	1.5	1.9

6.2 Influence of vapour diffusion

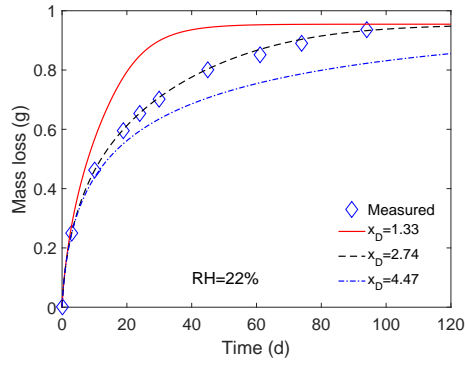
Theoretically, K_l should be independent of the external drying conditions. The previous study [8] argued that the discrepancy between K_l determined at different RHs was thought to be affected by the preparation of different specimens of the same mix design. Nonetheless, the batch effect is minimized in this study. One of possible reasons is that the effect of vapor diffusion varies with the drying condition, because it was found that vapor diffusion gradually becomes more important with the decrease of external RH [46]. In the above analysis, we assumed that $x_D = 2.74$ in Eq. (7) is suitable for all cases. To evaluate this assumption, we take different values for x_D (the main parameter controlling the rate of vapor diffusion) to simulate the drying mass loss curve: $x_D = 1.33$ was proposed by Millington and Quirk [52], $x_D = 2.74$ is suggested by Thiery et al. [82], and $x_D = 4.47$ is the value that we found for cementitious materials [8] based on calibration by the measured D_{eff} curve [6]. Results of three drying conditions are compared in Fig. 7. It is clear that the influence of x_D is closely related to the drying condition, as it is more significant for drying at low RHs. The influence decreases with the increase of external RH and eventually at RH = 63% the influence vanishes.

It was reported that x_D varies with materials [8] and a universal value that can be used for all cementitious materials could not be found. Since there is no generally accepted value for x_D , it is a good practice to choose the drying condition that has the negligible effect of vapor diffusion on the total mass loss. The goal here is to understand the range of RH under which the influence of vapor diffusion in the moisture transport model is negligible. Actually, this can be assessed by calculating the effective diffusion coefficient considering the moisture transport as a pure diffusion-like process. Based on Eqs. (1), (2) and (3), the effective diffusion coefficient D_{eff} is written as

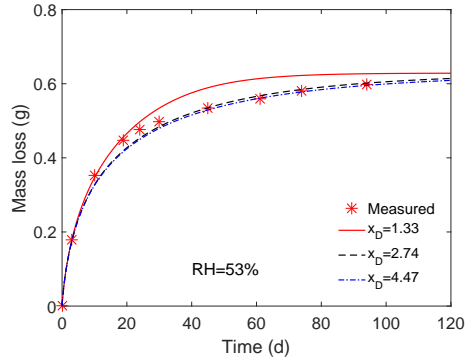
$$D_{eff} = k_{rl} \frac{K_l}{\phi \eta_l} \frac{dP_c}{dS} + \left(\frac{M_v}{\rho_l RT} \right)^2 D_{v0} f(S, \phi) \frac{P_{vs} RH}{\phi} \frac{dP_c}{dS} \quad (28)$$

The plot of D_{eff} vs. RH is shown in Fig. 8 which displays a bumpy curve with one peak at low RH and one at RH close to 1. The lowest point between them is found at RH \approx 43%, which is considered as the demarcation between the liquid and vapor transport. Below this point, vapor diffusion dominates the moisture transport; above this point, the advection of liquid becomes significant. Clearly, RH = 53% and 63% are located in the liquid water dominant region. However, RH = 53% is very close to the demarcation point and liquid transport is not considerably higher than vapor diffusion, so that we can still see the influence of x_D on the calculated mass loss curve (see Fig. 7b). From this point of view, we are able to say that K_l determined by the drying test at RH=63% is more accurate than values obtained by drying at lower RHs. Therefore, our recommendation is that if one wants to use the inverse analysis method to determine K_l , it is better to avoid using measured mass loss curves at low RHs (i.e., below the demarcation point on the effective diffusion coefficient curve).

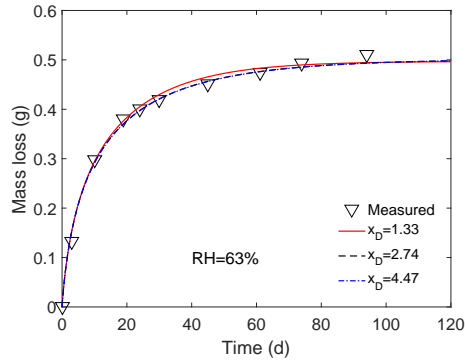
Another implication from this discussion is that an appropriate model that targets on the whole range of RH must include the contribution from both liquid and vapor. Some models in the literature that consider the effective diffusion coefficient/diffusivity as a monotonically increasing function with water content/degree of saturation are not suitable for moisture transport at low RHs, because they basically ignore the transport of water vapor.



(a) Drying at RH=22%.



(b) Drying at RH=53%.



(c) Drying at RH=63%.

Figure 7: Comparison of the effect of vapor diffusion on simulated mass loss. The case of $x_D = 4.47$ is used in this study to inversely determine K_l .

6.3 Overestimation of KC and KT equations

In agreement with most literature, this study finds that the KC and KT equations overestimate K_l of cement pastes. Halamickova et al. [83] pointed out that the KT relations may work better for systems with highly interconnected capillary pore networks than for systems where the fine nanostructure of gel pores dominates the transport, as is the case in most cementitious materials. This can help to explain why the permeability calculated by the KT equations is larger. Indeed, as originally explained by Katz and Thompson, their theory is valid for materials with large pores and mono-modal PSD centered in the capillary range [84].

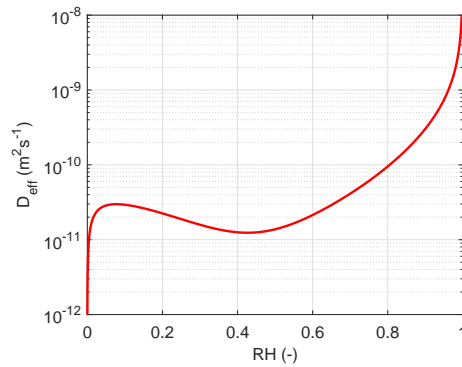


Figure 8: Calculated D_{eff} curve ($K_l = 1.9 \times 10^{-21} \text{ m}^2$ and $x_D = 2.74$). Note that D_{eff} is material-dependent and thus for other materials the shape of the curve should be different to the one in this figure.

In addition to the inherent reasons, there are some deficiencies in the measured data for KC and KT equations:

- 1) The data used in these equations are measured by MIP, which is not sensitive to the small pores. Pores in hydrated materials can be generally divided into capillary pores and gel pores. Capillary pores are easily detected by MIP, but not gel pores, whose contribution to the permeability of cementitious materials is non-negligible [75]. The contribution of small pores to the PSD is not fully included in MIP data and therefore measured surface area is much lower than other techniques, so that it leads to a higher K_l in the KC equation.
- 2) Another basic problem with MIP is that the specimens are dried before measurements. As pointed out in the literature, the microstructure of the material is altered whatever the selected method for drying (oven-drying, vacuum drying, freezing drying or solvent exchange) [72]. The different measured PSD curves for two drying methods in the present study also show that the pretreatment conditions have an influence on the measured PSD.
- 3) The choice of the critical diameter also contributes the difference. The critical pore diameter was defined as the pore size above which a connected path can form from one side of the specimen to the opposite side. It is reflected by the inflection point of the cumulative mercury intrusion curve. The determination of the critical diameter holds an accuracy of $\pm 15\%$ [67]. According to the definition of the critical diameter, it is most likely the characteristic pore diameter of gel pores d_{gp} , which is much smaller than d_c [85]. If d_{gp} is used in Eqs. (23) and (26), the predicted permeability should be about one or two orders of magnitudes lower, and much closer to the values from the BB and inverse analysis methods. However, the choice is not arbitrary and is controlled by the critical porosity ϕ_c which varies with materials.

Hence, if the measured microstructure is more representative of the original one, it is expected to yield more accurate K_l . Experimental methods that can measure the PSD of the saturated specimen are suggested for the future studies, such as nuclear magnetic resonance (NMR) and thermoporometry.

6.4 Permeability measured by other fluids

The permeability is often measured by other gases and liquids in the literature. For gas permeability measurements, specimens must be dried or partially dried. The problem is that the morphology of C-S-H can be significantly changed by drying. By observing under the environmental scanning electron microscope (ESEM), Fonseca and Jennings [77] reported that a slow drying, such as drying at high RH for several days, creates a bumpy morphology around the cement grain, which is very different to the needle-like structure in the rapidly dried specimens. Based on the comparison of different drying methods, Zhang and Scherer [71] and Zhang et al. [69] found that no matter which drying method is used, as long as water is removed from the pore network, the morphology of hydration products is altered and thin sheets between fine fibers are created. These effects, either forming bumpy surface or creating thin sheets, will increase the complexity of the microstructure. Together with coarsening the pore size distribution (e.g., [9]) and inducing micro-cracks (e.g., [86]), the transport properties would be affected. Therefore, we should not directly compare permeabilities measured by water with that by gases, because the microstructure of the specimens is different to each other.

Loosveldt et al. [10] found that water permeability was systematically lower (by 1 - 2 orders of magnitudes) than that of argon gas, and ethanol permeability was between them. A similar conclusion was reported by Zhou et al. [12] that ethanol permeability is about 2 - 3 orders of magnitudes higher than water permeability and close to the gas permeability with the correction of Klinkenberg slippage effect. However, these results are questionable. First, ethanol has been proved to react with hydration products (essentially calcium hydroxide) [72]. Second, ethanol permeability was measured after gas permeability measurements on the same specimen. As mentioned above, the microstructure of dried specimen has been altered compared to the original water-saturated one. A more acceptable way is to do solvent exchange with the water-saturated specimen before measuring the solvent permeability. By using this procedure, Hearn [11] reported that there is only slight difference between water and IPA permeabilities. The difference is due to water having stronger chemical interactions than IPA with the hydration products. Nevertheless, recent studies by Zhou et al. [9] reported that IPA permeability is about 2 - 3 orders of magnitudes higher than water permeability. They found that the peaks of PSD measured by NMR shift to high pore size range for IPA treated specimens, meaning that the microstructure is coarsened by IPA replacement. It is hard to believe that IPA replacement causes permeability 2 - 3 orders of magnitudes higher than the one measured with water saturated specimen since IPA replacement was shown as a preferable drying method to preserve the microstructure [87, 88, 72, 69]. The most possible reason is that some microcracks are induced during solvent exchange as reported in our previous study [71] that the damage is more serious for a large specimen (≥ 8 mm in diameter). The thickness of the specimen in [9] is 20 - 25 mm, so damages most likely happened during exchanging with IPA. Another fact that can lead to damage during IPA replacement is the exchange duration. Vichit-Vadakan and Scherer [28] reported that after about a 6-week exchange the measured porosity of cement paste dramatically increased to the same value as the oven dried specimen at 105 °C, and they suspected damages because of the long exchange duration.

7 Conclusion

To eliminate the artifacts (e.g., types of cements, specimen preparation and curing conditions) in the measurement of water permeability, this study prepared all specimens from a long cylinder for a variety of permeability determination methods. specimens from the same cylinder were also used for experiments to obtain the input and calibration data for a moisture transport model. By comparing the simulated and measured mass loss curves, we found that the KC, KTII and sorptivity methods yield significantly greater values of K_l which lead to overestimation of the mass loss. Permeability determined by the BB method provides a mass loss curve slightly lower than measured one, but it is the closest one among the compared methods.

The overestimation of the KC, KTII and sorptivity methods results from the fact that specimens used in these methods must be dried before the tests. As shown in our previous studies, any drying (either fully or partially) can significantly alter the microstructure of the material. In addition, MIP is not an appropriate method to detect the small pores in cementitious materials; thus, the measured surface area and critical pore size are far from the “true” ones in the water-saturated specimen. In addition, by comparing sorptivity measurements for different initial water content, we found that the use of specimens with high initial water content is inappropriate for the sorptivity method.

The permeability values inversely determined by the moisture transport model based on the measured mass loss curves are very close to those measured by the beam-bending method. The most important notice put forward in this study for the use of the inverse analysis method is that drying tests must be done at high RHs (63% in this study) to reduce the effect of vapor diffusion on the determination of water permeability.

This study has tried to minimize the batch effect, but permeabilites determined by a variety of methods are still much different to each other. This may indicate that the effect of choosing the water permeability determination method is more important than eliminating the batch effect.

Acknowledgment

ZZ would like to thank Professor Chunsheng Zhou from HIT for discussion of using sorptivity method to determine permeability.

References

- [1] K. Hong, R. D. Hooton, Effects of cyclic chloride exposure on penetration of concrete cover, *Cement and Concrete Research* 29 (1999) 1379–1386. doi : 10.1016/S0008-8846(99)00073-3.
- [2] M. Mainguy, O. Coussy, V. Baroghel-Bouny, Role of air pressure in drying of weakly permeable materials, *Journal of Engineering Mechanics* 127 (2001) 582–592.
- [3] Z. Zhang, M. Thiéry, V. Baroghel-Bouny, Analysis of moisture transport in cementitious materials and modelling of drying-wetting cycles, in: *International Conference: Numerical Modeling Strategies for Sustainable Concrete Structures*, The French Association of Civil Engineering (AFGC), Aix-en-Provence, France, 2012, pp. I-5 FP 277.

- [4] O. Coussy, *Mechanics and physics of porous solids*, John Wiley & Sons, Ltd, United Kingdom, 2010.
- [5] O. Coussy, M. Thiéry, *Asymptotic*, in: *Poro-Mechanics IV*, Ed. by Hoe I. Ling and Andrew Smyth, DEStech Publications, Inc., Lancaster, USA, 2009, pp. 384–389.
- [6] V. Baroghel-Bouny, *Water vapour sorption experiments on hardened cementitious materials. Part II: Essential tool for assessment of transport properties and for durability prediction*, *Cement and Concrete Research* 37 (2007) 438–454.
- [7] Z. Zhang, M. Thiery, V. Baroghel-Bouny, *Numerical modelling of moisture transfers with hysteresis within cementitious materials: Verification and investigation of the effects of repeated wetting–drying boundary conditions*, *Cement and Concrete Research* 68 (2015) 10–23.
- [8] Z. Zhang, M. Thiery, V. Baroghel-Bouny, *Investigation of moisture transport properties of cementitious materials*, *Cement and Concrete Research* 89 (2016) 257–268.
- [9] C. Zhou, F. Ren, Z. Wang, W. Chen, W. Wang, *Why permeability to water is anomalously lower than that to many other fluids for cement-based material?*, *Cement and Concrete Research* 100 (2017) 373–384.
- [10] H. Loosveldt, Z. Lafhaj, F. Skoczylas, *Experimental study of gas and liquid permeability of a mortar*, *Cement and Concrete Research* 32 (2002) 1357–1363.
- [11] N. Hearn, *Comparison of water and propan-2-ol permeability in mortar specimens*, *Advances in Cement Research* 8 (1996) 81–86.
- [12] C. Zhou, W. Chen, W. Wang, F. Skoczylas, *Indirect assessment of hydraulic diffusivity and permeability for unsaturated cement-based material from sorptivity*, *Cement and Concrete Research* 82 (2016) 117–129.
- [13] B. K. Nyame, J. M. Illston, *Relationships between permeability and pore structure of hardened cement paste*, *Magazine of Concrete Research* 33 (1981) 139–146.
- [14] N. Hearn, *Recording permeameter for measuring time-sensitive permeability of concrete*, *Ceramic Transactions-Advances in Cementitious Materials* 16 (1990) 467–475.
- [15] A. S. El-Dieb, R. D. Hooton, *Water-permeability measurement of high performance concrete using a high-pressure triaxial cell*, *Cement and Concrete Research* 25 (1995) 1199–1208.
- [16] L. Bágel, V. Živica, *Relationship Between Pore Structure and Permeability of Hardened Cement Mortars: on the Choice of Effective Pore Structure Parameter*, *Cement and Concrete Research* 27 (8) (1997) 1225–1235.
- [17] G. Ye, *Percolation of capillary pores in hardening cement pastes*, *Cement and Concrete Research* 35 (2005) 167–176.
- [18] Q. T. Phung, N. Maes, G. De Schutter, D. Jacques, G. Ye, *Determination of water permeability of cementitious materials using a controlled constant flow method*, *Construction and Building Materials* 47 (2013) 1488–1496.

- [19] Z. Kameche, F. Ghomari, M. Choinska, A. Khelidj, Assessment of liquid water and gas permeabilities of partially saturated ordinary concrete, *Construction and Building Materials* 65 (2014) 551–565.
- [20] W. Brace, J. Walsh, W. Frangos, Permeability of granite under high pressure, *Journal of Geophysical research* 73 (6) (1968) 2225–2236.
- [21] C. A. Jones, Z. C. Grasley, Correlation of radial flow-through and hollow cylinder dynamic pressurization test for measuring permeability, *Journal of Materials in Civil Engineering* 21 (10) (2009) 594–600.
- [22] J. L. Rose, Z. C. Grasley, Comparison of permeability of cementitious materials obtained via poromechanical and conventional experiments, *Journal of Materials in Civil Engineering* 29 (9) (2017) 04017083.
- [23] A. Amriou, M. Bencheikh, New experimental method for evaluating the water permeability of concrete by a lateral flow procedure on a hollow cylindrical test piece, *Construction and Building Materials* 151 (2017) 642–649.
- [24] G. W. Scherer, Dynamic pressurization method for measuring permeability and modulus: I. theory, *Materials and Structures* 39 (2006) 1041–1057.
- [25] Z. C. Grasley, G. W. Scherer, D. A. Lange, J. J. Valenza, Dynamic pressurization method for measuring permeability and modulus: II. cementitious materials, *Materials and Structures* 40 (2007) 711–721.
- [26] G. W. Scherer, Bending of gel beams: method of characterizing mechanical properties and permeability, *Journal of Non-Crystalline Solids* 142 (1992) 18–35.
- [27] G. W. Scherer, Measuring permeability of rigid materials by a beam-bending method: I. theory, *Journal of the American Ceramic Society* 83 (2000) 2231–2239, erratum, *J. Am. Ceram. Soc.* 87 [8] (2004) 1612-1613.
- [28] W. Vichit-Vadakan, G. W. Scherer, Measuring permeability of rigid materials by a Beam-Bending Method: III, cement paste, *Journal of the American Ceramic Society* 85 (6) (2002) 1537–1544.
- [29] W. Vichit-Vadakan, G. W. Scherer, Measuring permeability and stress relaxation of young cement paste by beam bending, *Cement and Concrete Research* 33 (12) (2003) 1925–1932.
- [30] G. W. Scherer, H. Hdach, J. Phalippou, Thermal expansion of gels: a novel method for measuring permeability, *Journal of Non-Crystalline Solids* 130 (1991) 157–170, errata, *J. Non-Cryst. Solids* 194 (1996) 326.
- [31] G. W. Scherer, Measuring permeability by the thermal expansion method for rigid or highly permeable gels, *Journal of Sol-Gel Science and Technology* 3 (1994) 31–40.
- [32] G. W. Scherer, Thermal expansion kinetics: method to measure permeability of cementitious materials: I, theory, *Journal of the American Ceramic Society* 83 (2000) 2753–2761, erratum, *Journal of the American Ceramic Society* 87 (8) (2004) 1609 –1610.

- [33] H. Ai, J. F. Young, G. W. Scherer, Thermal expansion kinetics: Method to measure permeability of cementitious materials: II, application to hardened cement pastes, *Journal of the American Ceramic Society* 84 (2001) 385–391.
- [34] G. W. Scherer, Poromechanics analysis of a flow-through permeameter with entrapped air, *Cement and Concrete Research* 38 (3) (2008) 368–378.
- [35] M. T. Nguyen, Modélisation des couplages entre hydratation et dessiccation des matériaux cimentaires à l’issue du décoffrage, Ph.D. thesis, ENPC (September 2009).
- [36] Z. Wu, H. Wong, N. Buenfeld, Influence of drying-induced microcracking and related size effects on mass transport properties of concrete, *Cement and Concrete Research* 68 (2015) 35–48.
- [37] J. Kozeny, Ueber kapillare leitung des wassers im boden, *Sitzungsber Akad. Wiss., Wien* 136 (1927) 271–306.
- [38] P. Carman, Fluid flow through granular beds, *Transactions* 15 (1937) 150–166.
- [39] P. Carman, Flow of gases through porous media, Butterworths, London, 1956.
- [40] T. Lambe, R. Whitman, Soil Mechanics, John Wiley & Sons Inc., New York, 1969.
- [41] H. Wong, N. Buenfeld, M. Head, Estimating transport properties of mortars using image analysis on backscattered electron images, *Cement and Concrete Research* 36 (8) (2006) 1556–1566.
- [42] A. Katz, A. Thompson, Quantitative prediction of permeability in porous rock, *Physical review B* 34 (11) (1986) 8179.
- [43] A. Katz, A. Thompson, Prediction of rock electrical conductivity from mercury injection measurements, *Journal of Geophysical Research: Solid Earth* 92 (B1) (1987) 599–607.
- [44] V. Baroghel-Bouny, K. Kinomura, M. Thiéry, S. Moscardelli, Easy assessment of durability indicators for concretes with high volume of scms, *Cement and Concrete Composites* 33 (2011) 832–847.
- [45] A. S. El-Dieb, D. Hooton, Evaluation of the katz-thompson model for estimating the water permeability of cement-based materials from mercury intrusion porosimetry data, *Cement and Concrete Research* 24 (1994) 443–455.
- [46] Z. Zhang, M. Thiery, V. Baroghel-Bouny, An equation for drying kinetics of cementitious materials, *Drying Technology* doi:10.1080/07373937.2017.1408644.
- [47] V. Baroghel-Bouny, Water vapour sorption experiments on hardened cementitious materials. Part I: Essential tool for analysis of hygral behaviour and its relation to pore structure, *Cement and Concrete Research* 37 (3) (2007) 414 – 437.
- [48] Z. Zhang, M. Thiery, V. Baroghel-Bouny, A review and statistical study of existing hysteresis models for cementitious materials, *Cement and Concrete Research* 57 (2014) 44–60.

- [49] M. T. van Genuchten, A closed-form equation for predicting the hydraulic conductivity of unsaturated soils, *Soil Science Society of America Journal* 44 (1980) 892–898.
- [50] S. D. Pont, F. Meftah, B. A. Schrefler, Modeling concrete under severe conditions as a multi-phase material, *Nuclear Engineering and Design* 241 (2011) 562–572.
- [51] M. Azenha, K. Maekawa, T. Ishida, R. Faria, Drying induced moisture losses from mortar to the environment. Part II: numerical implementation, *Materials and Structures* 40 (2007) 813–825.
- [52] R. Millington, J. Quirk, Permeability of porous solids, *Transactions of the Faraday Society* 57 (1961) 1200–1207.
- [53] M. Thiéry, P. Belin, V. Baroghel-Bouny, M. D. Nguyen, Modelling of isothermal drying process in cementitious materials – Analysis of the moisture transfer and proposal of simplified approaches, in: *Proceedings of 3rd International Conference on Coupled T-H-M-C Processes in Geo-systems*, Polytech Lille, France, 2008, pp. 571–581.
- [54] V. Papadakis, C. Vayenas, M. Fardis, Physical and chemical characteristics affecting the durability of concrete, *ACI Materials Journal* 8 (1991) 186–196.
- [55] Y. Mualem, A new model for predicting the hydraulic conductivity of unsaturated porous media, *Water Resources Research* 12 (1976) 513–522.
- [56] J. C. Parker, R. J. Lenhard, A model for hysteretic constitutive relations governing multiphase flow: 1. Saturation-pressure relations, *Water Resources Research* 23 (1987) 2187–2196.
- [57] S. Zamani, R. Kowalczyk, P. J. McDonald, The relative humidity dependence of the permeability of cement paste measured using garfield nmr profiling, *Cement and Concrete Research* 57 (2014) 88–94.
- [58] J. R. Philip, The theory of infiltration: 4. sorptivity and algebraic infiltration equations, *Soil Science* 84 (1957) 257–264.
- [59] C. Hall, W. D. Hoff, *Water transport in brick, stone and concrete* (2nd edition), CRC Press, Boca Raton FL, 2011.
- [60] J. Philip, General method of exact solution of the concentration-dependent diffusion equation, *Australian Journal of Physics* 13 (1960) 1–12.
- [61] W. Brutsaert, The concise formulation of diffusive sorption of water in a dry soil, *Water Resources Research* 12 (6) (1976) 1118–1124.
- [62] J.-Y. Parlange, D. Barry, M. Parlange, D. Lockington, R. Haverkamp, Sorptivity calculation for arbitrary diffusivity, *Transport in porous media* 15 (3) (1994) 197–208.
- [63] C. Zhou, General solution of hydraulic diffusivity from sorptivity test, *Cement and Concrete Research* 58 (2014) 152–160.
- [64] D. Lockington, J.-Y. Parlange, P. Dux, Sorptivity and the estimation of water penetration into unsaturated concrete, *Materials and Structures* 32 (5) (1999) 342.

- [65] C. Zhou, Predicting water permeability and relative gas permeability of unsaturated cement-based material from hydraulic diffusivity, *Cement and Concrete Research* 58 (2014) 143–151.
- [66] V. Sánchez-Fajardo, M. Torres, A. Moreno, Study of the pore structure of the lightweight concrete block with lapilli as an aggregate to predict the liquid permeability by dielectric spectroscopy, *Construction and Building Materials* 53 (2014) 225–234.
- [67] H. Ma, Mercury intrusion porosimetry in concrete technology: tips in measurement, pore structure parameter acquisition and application, *Journal of porous materials* 21 (2) (2014) 207–215.
- [68] J. Walsh, W. Brace, The effect of pressure on porosity and transport properties of rock, *Journal of Geophysical Research* 89 (1984) 9425–9431.
- [69] Z. Zhang, G. W. Scherer, A. Bauer, Morphology of cementitious material during early hydration, *Cement and Concrete Research* (2017).
- [70] J. Zhang, G. W. Scherer, Permeability of shale by the beam-bending method, *International Journal of Rock Mechanics and Mining Sciences* 53 (2012) 179–191.
- [71] Z. Zhang, G. W. Scherer, Supercritical drying of cementitious materials, *Cement and Concrete Research* 99 (2017) 137–154.
- [72] J. Zhang, G. W. Scherer, Comparison of methods for arresting hydration of cement, *Cement and Concrete Research* 41 (2011) 1024–1036.
- [73] Z. Sun, G. W. Scherer, Pore size and shape in mortar by thermoporometry, *Cement and Concrete Research* 40 (5) (2010) 740–751.
- [74] G. Constantinides, F.-J. Ulm, The effect of two types of csh on the elasticity of cement-based materials: Results from nanoindentation and micromechanical modeling, *Cement and concrete research* 34 (1) (2004) 67–80.
- [75] G. W. Scherer, J. J. V. II, G. Simmons, New methods to measure liquid permeability in porous materials, *Cement and Concrete Research* 37 (2007) 386–397.
- [76] J. J. Thomas, H. M. Jennings, A. J. Allen, The surface area of hardened cement paste as measured by various techniques, *Concrete Science and Engineering* 1 (1) (1999) 45–64.
- [77] P. Fonseca, H. Jennings, The effect of drying on early-age morphology of C–S–H as observed in environmental SEM, *Cement and Concrete Research* 40 (2010) 1673–1680.
- [78] O. Coussy, V. Baroghel-Bouny, P. Dangla, M. Mainguy, Assessment of the water permeability of concretes from their mass loss during drying (in french), in: V. Baroghel-Bouny (Ed.), *Transferts dans les bétons et durabilité*, Special issue of *Revue Française de Génie Civil*, vol. 5, Hermès Science Publications, Paris, 2001, pp. 269–284.
- [79] V. Baroghel-Bouny, M. Thiéry, F. Barberon, O. Coussy, G. Villain, Assessment of transport properties of cementitious materials. A major challenge as regards durability?, *Revue European de Genie Civil* 11 (2007) 671–696.

- [80] H. M. Jennings, Refinements to colloid model of csh in cement: Cm-ii, *Cement and Concrete Research* 38 (3) (2008) 275–289.
- [81] N. Fischer, R. Haerdtl, P. McDonald, Observation of the redistribution of nanoscale water filled porosity in cement based materials during wetting, *Cement and Concrete Research* 68 (2015) 148–155.
- [82] M. Thiery, V. Baroghel-Bouny, N. Bourneton, G. Villain, C. Stéfani, Modélisation du séchage des bétons - Analyse des différents modes de transfert hydrique, *Revue européenne de génie civil* 11 (2007) 541–577.
- [83] P. Halamickova, R. J. Detwiler, D. P. Bentz, E. J. Garboczi, Water permeability and chloride ion diffusion in portland cement mortars: Relationship to sand content and critical pore diameter, *Cement and Concrete Research* 25 (1995) 790–802.
- [84] D. L. Johnson, J. Koplik, L. M. Schwartz, New pore-size parameter characterizing transport in porous media, *Physical Review Letters* 57 (1986) 2564–2567.
- [85] K. K. Aligizaki, *Pore structure of cement-based materials: testing, interpretation and requirements*, Taylor & Francis, London and New York, 2006.
- [86] C. de Sa, F. Benboudjema, M. Thiery, J. Sicard, Analysis of microcracking induced by differential drying shrinkage, *Cement and Concrete Composites* 30 (10) (2008) 947–956.
- [87] L. Konecny, S. J. Naqvi, The effect of different drying techniques on the pore size distribution of blended cement mortars, *Cement and Concrete Research* 23 (1993) 1223–1228.
- [88] J.J.Beaudoin, Validity of using methanol for studying the microstructure of cement paste, *Materials and Structures* 20 (1987) 27–31.